Int. J. Electrochem. Sci., 8 **(2013)** 3664 - 3675

International Journal of
ELECTROCHEMICAL
SCIENCE
www.electrochemsci.org

Electrochemical Properties of Nanosized $Li_2MnO_3 \cdot Li(Ni_{0.8}Co_{0.15}Al_{0.05})O_2$ Composite Cathode Powders

Jung Hyun Kim, Yun Chan Kang[*]

Department of Chemical Engineering, Konkuk University, 1 Hwayang-dong, Gwangjin-gu, Seoul 143-701, Korea
*E-mail: yckang@konkuk.ac.kr

Received: 9 January 2013 / *Accepted:* 6 February 2013 / *Published:* 1 March 2013

Nanometer-sized $LiNi_{0.8}Co_{0.15}Al_{0.05}O_2$ and $0.6Li_2MnO_3 \cdot 0.4LiNi_{0.8}Co_{0.15}Al_{0.05}O_2$ powders are prepared by high-temperature flame spray pyrolysis. The $0.6Li_2MnO_3 \cdot 0.4LiNi_{0.8}Co_{0.15}Al_{0.05}O_2$ composite powders post-treated at 700 and 800°C exhibit mixed-layer crystal structures comprising layered Li_2MnO_3 and layered $LiNi_{0.8}Co_{0.15}Al_{0.05}O_2$ phases. The mean sizes of the composite powders post-treated at 700 and 800°C are 127 and 180 nm, respectively. The layered–layered composite powders have sizes in the nanometer range with a slightly aggregated structure, whereas the layered $LiNi_{0.8}Co_{0.15}Al_{0.05}O_2$ powders have sizes in micrometer range with a hardly aggregated structure. The discharge capacity of the $LiNi_{0.8}Co_{0.15}Al_{0.05}O_2$ powders decreases from 163 to 95 mAh g^{-1} after 50 cycles with a capacity retention of 58%. The discharge capacity of the $0.6Li_2MnO_3 \cdot 0.4LiNi_{0.8}Co_{0.15}Al_{0.05}O_2$ composite powders decreases from 235 to 200 mAh g^{-1} after 50 cycles with a capacity retention of 85%.

Keywords: cathode material; flame spray pyrolysis; composite material; lithium-rich material; nanomaterials

1. INTRODUCTION

The properties of cathode powders such as morphology, mean size, specific surface area, crystallinity, and composition have an effect on the electrochemical performance of the corresponding cathodes in lithium ion batteries [1-5]. Improved electrochemical performance of the cathode may be derived by enabling rapid Li^+ ion diffusion. The rate of lithium insertion/extraction is significantly increased as the diffusion path length of the lithium ions is significantly reduced [6], and hence, an effective means for enhancing the rate of Li^+ diffusion is by using nanomaterials in cathodes [7]. Recently, Li_2MnO_3-stabilized cathodes with composite structures have become attractive because of their high discharge capacity of over 200 mAh g^{-1} and enhanced safety at high voltages over 4.5 V [8-

18]. Conventional solid-state reaction processes are normally used to synthesize transition metal oxide cathode materials [10,19,20]. However, it is difficult to produce nanometer-sized cathode powders using a solid-state reaction process because of the long calcination time at high temperatures that is required [19].

Flame spray pyrolysis is a widely used technique for synthesizing a number of functional powders over a range of sizes from nanometers to micrometers [21,22]. In flame spray pyrolysis, aggregation-free cathode nanopowders were directly prepared inside a high-temperature diffusion flame [23-27]. In this study, nanosized $LiNi_{0.8}Co_{0.15}Al_{0.05}O_2$ and $0.6Li_2MnO_3 \cdot 0.4LiNi_{0.8}Co_{0.15}Al_{0.05}O_2$ composite powders were prepared by high-temperature flame spray pyrolysis. The morphologies and electrochemical properties of the prepared layered–layered composite powders were compared to those of the layered cathode powders.

2. EXPERIMENTAL

The flame spray pyrolysis system employed had a droplet generator, a flame nozzle, a quartz reactor, a powder collector, and a blower. A 1.7 MHz ultrasonic spray generator with six resonators was used to generate droplets, which were then carried into the high-temperature diffusion flame by oxygen (carrier gas) [20]. Propane (fuel) and oxygen (oxidizer) were used to produce the diffusion flame. The flow rate of the fuel gas was 5 L min^{-1}, and those of the oxidizer and carrier gases were 40 and 10 L min^{-1}, respectively. The starting materials used for the synthesis were $LiNO_3$ (Junsei, 98%), $Ni(NO_3)_2 \cdot 6H_2O$ (Junsei, 98%), $Mn(CH_3COO) \cdot 4H_2O$ (Junsei, 97%), $Co(NO_3)_2 \cdot 6H_2O$ (Junsei, 97%), and $Al(NO_3)_3 \cdot 9H_2O$ (Junsei, 98%). The overall concentration of the metal components in the solution was 0.5 M. The amount of excess lithium in the solution was 20% of the stoichiometric amount. The as-prepared powders obtained by flame spray pyrolysis were post-treated at temperatures of 700 and 800°C under an oxygen atmosphere.

The crystal structures of the post-treated powders were investigated through X-ray diffractometry (XRD, Rigaku DMAX-33) using Cu Kα radiation at the Korea Basic Science Institute (Daegu). The morphological characteristics of the powders were investigated using scanning electron microscopy (SEM, JEOL, JSM-6060) and transmission electron microscopy (TEM, JEOL, JEM-2010). The electrode was fabricated using a mixture of 80 wt% of $LiNi_{0.8}Co_{0.15}Al_{0.05}O_2$ powders or $0.6Li_2MnO_3 \cdot 0.4LiNi_{0.8}Co_{0.15}Al_{0.05}O_2$ composite powders; 10 wt% carbon black (Super-P), as a conductive material; and 10 wt% polytetrafluoroethylene (PTFE), as a binder, with a few drops of alcohol. Lithium metal and a microporous polypropylene film were used as the counter electrode and separator, respectively. The electrolyte was 1 M $LiPF_6$ in a 1:1 mixture (by volume) of ethylene carbonate/dimethyl carbonate (EC/DMC). The entire cell was assembled in a glove box in an argon atmosphere. The charge/discharge characteristics of the samples were determined by cycling in the potential range 2–4.8 V at a constant current density of 20 mA g^{-1} using a coin cell (2032 type).

3. RESULTS AND DISCUSSION

The morphologies of the powders prepared by flame spray pyrolysis were affected by the type of solvent used and the flow rates of the fuel, oxidizer, and carrier gases. Ethyl alcohol was added to the spray solution to improve the temperature of the diffusion flame. In the mixed solvent, the volume ratio of ethyl alcohol to distilled water was 3:7. An increase in the flow rate of the fuel gas causes an increase in the temperature and length of the diffusion flame. The flow rate of the oxidizer gas should therefore be optimized to obtain a high-temperature diffusion flame with complete combustion of the fuel gas.

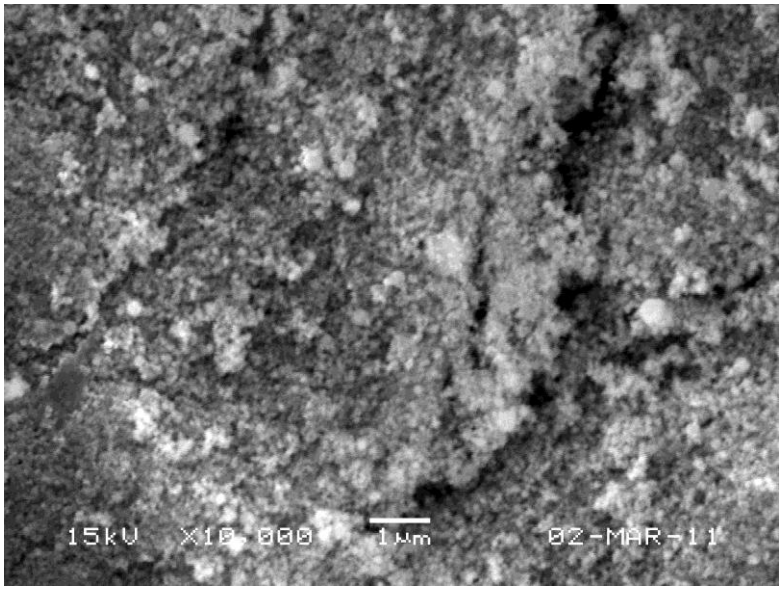

(a) $LiNi_{0.8}Co_{0.15}Al_{0.05}O_2$

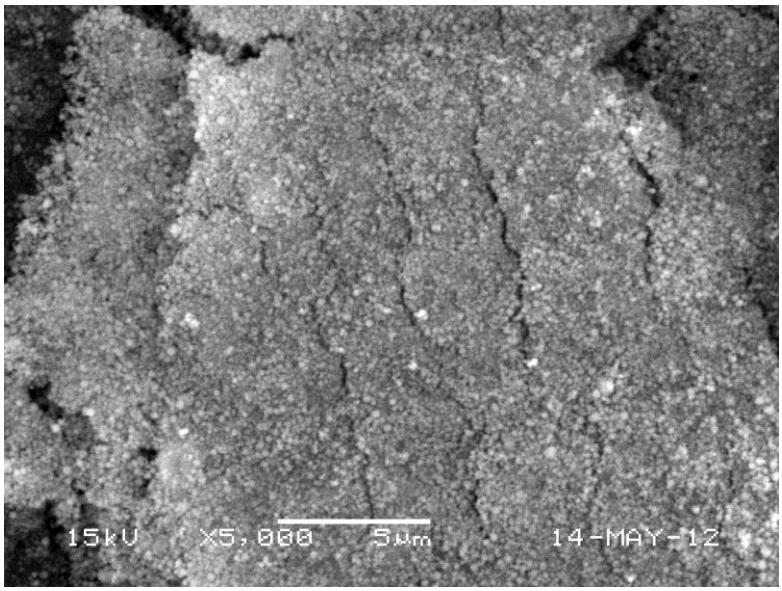

(b) $0.6Li_2MnO_3$-$0.4LiNi_{0.8}Co_{0.15}Al_{0.05}O_2$

Figure 1. SEM images of the $LiNi_{0.8}Co_{0.15}Al_{0.05}O_2$ and $0.6Li_2MnO_3$-$0.4LiNi_{0.8}Co_{0.15}Al_{0.05}O_2$ composite powders prepared directly by flame spray pyrolysis.

The flow rate of the carrier gas will determine the residence time of the powders inside the diffusion flame. The flow rates of the fuel, oxidizer, and carrier gases were optimized for the flame spray pyrolysis process in this study, and the estimated values of flow rates were 5, 40, and 10 L min^{-1}, respectively. The morphologies of the $LiNi_{0.8}Co_{0.15}Al_{0.05}O_2$ and $0.6Li_2MnO_3 \cdot 0.4LiNi_{0.8}Co_{0.15}Al_{0.05}O_2$ powders prepared directly by flame spray pyrolysis are shown in Fig. 1.

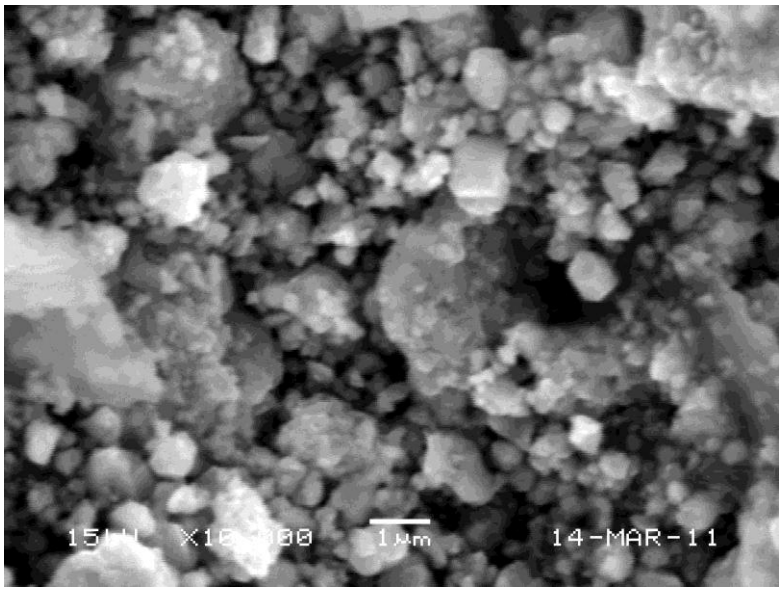

(a) SEM

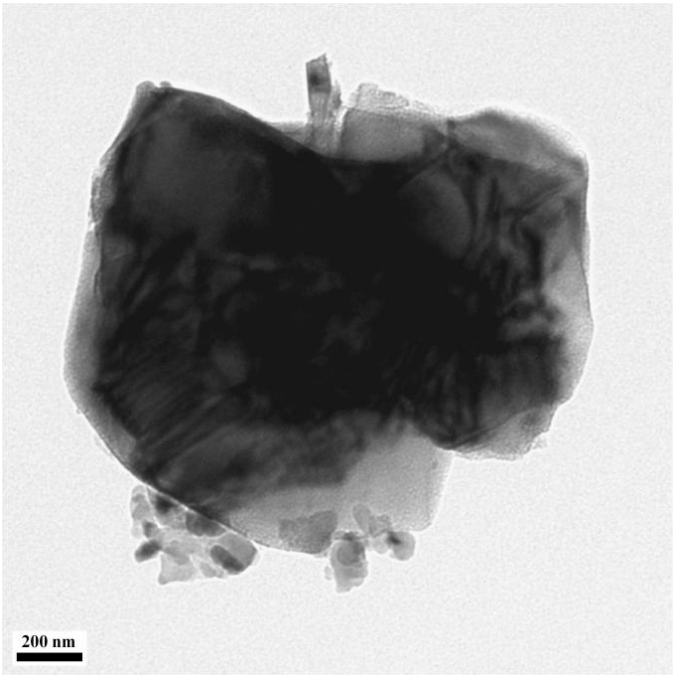

(b) TEM

Figure 2. SEM and TEM images of the $LiNi_{0.8}Co_{0.15}Al_{0.05}O_2$ powders post-treated at 700°C.

All the powder prepared by flame spray pyrolysis comprised nanometer-sized particles. Complete evaporation of the lithium, manganese, nickel, cobalt, and aluminum components occurred inside the high-temperature diffusion flame, resulting in the nanometer-sized $LiNi_{0.8}Co_{0.15}Al_{0.05}O_2$ and $0.6Li_2MnO_3 \cdot 0.4LiNi_{0.8}Co_{0.15}Al_{0.05}O_2$ powders through nucleation and growth processes from the evaporated vapors.

To improve the crystallinity and remove possible impurity phases, the as-prepared powders obtained by flame spray pyrolysis were post-treated at a temperature of 700°C for 5 h under oxygen atmosphere. Fig. 2 shows the SEM and TEM images of the post-treated layered $LiNi_{0.8}Co_{0.15}Al_{0.05}O_2$ powders. After post-treatment process, the nanometer-sized $LiNi_{0.8}Co_{0.15}Al_{0.05}O_2$ powders prepared by flame spray pyrolysis turned into micron-sized powders with hard aggregation between the powders. Extensive aggregation between the powders can lead to the poor electrochemical performance of the cathode powders.

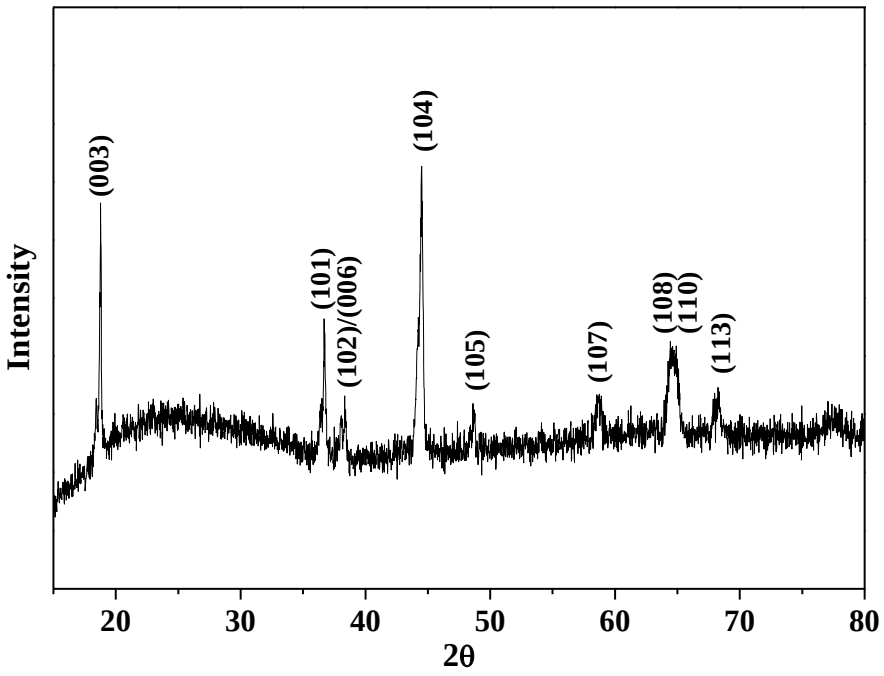

Figure 3. XRD pattern of the $LiNi_{0.8}Co_{0.15}Al_{0.05}O_2$ powders post-treated at 700°C.

The XRD pattern of the layered $LiNi_{0.8}Co_{0.15}Al_{0.05}O_2$ powders post-treated at 700°C is shown in Fig. 3. The peaks corresponding to the $LiNi_{0.8}Co_{0.15}Al_{0.05}O_2$ powders can be indexed to a hexagonal α-$NaFeO_2$ structure. The peak separations of the (006)/(102) and (108)/(110) peaks in the XRD pattern, indicative of a layered structure and good electrochemical properties, were not clearly observed. This result suggests that a post-treatment temperature higher than 700°C was required to improve the crystallinity and electrochemical properties of the $LiNi_{0.8}Co_{0.15}Al_{0.05}O_2$ powders. However, a high post-treatment temperature leads to increase in particle sizes to micron level and more extensive aggregation between the powders.

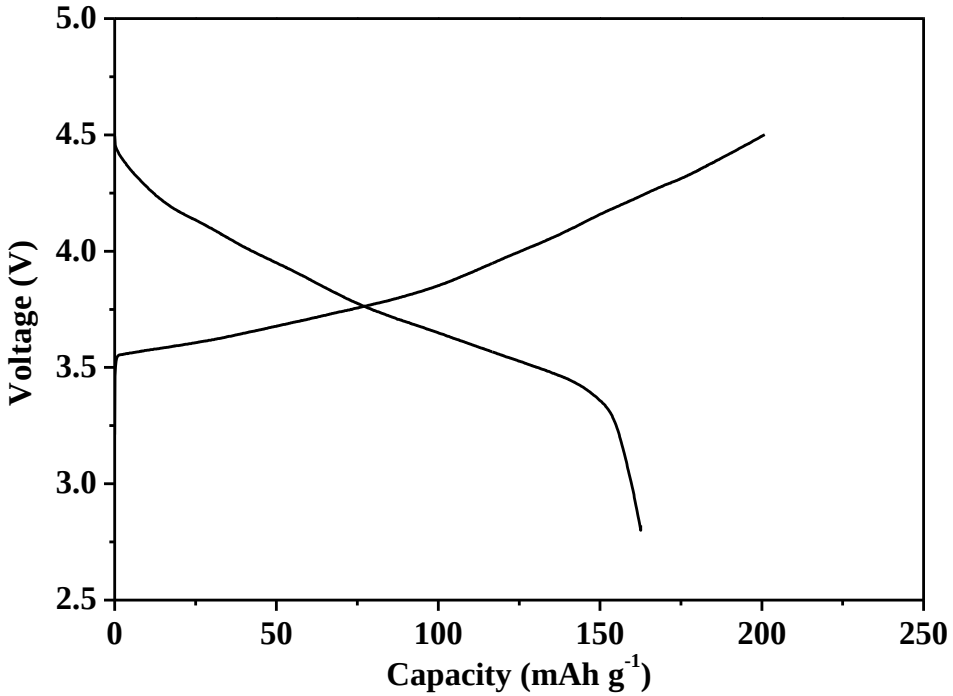

(a) Initial charge/discharge curves

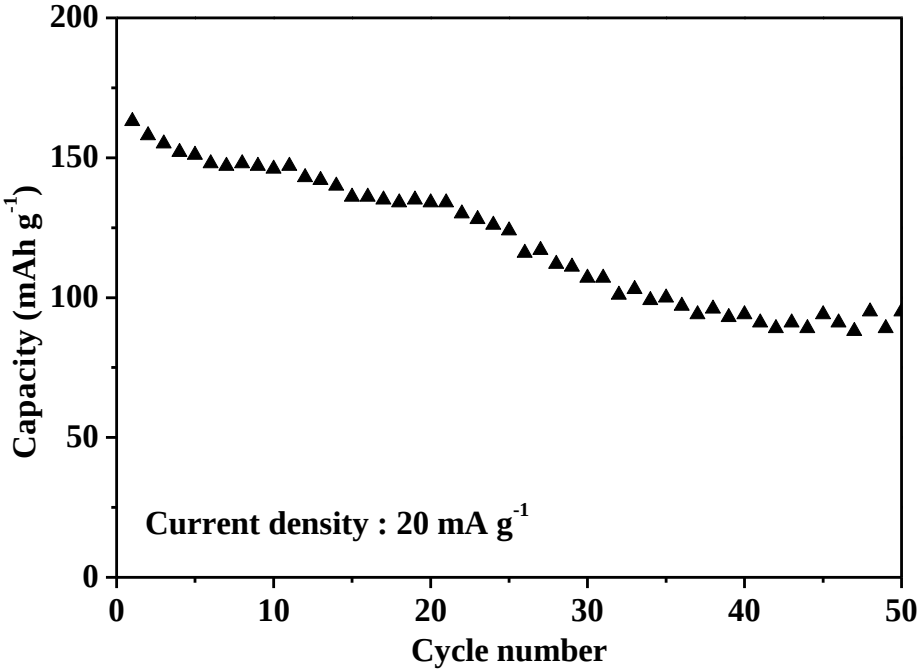

(b) Cycling performance

Figure 4. Initial charge/discharge curves and cycling performance of the $LiNi_{0.8}Co_{0.15}Al_{0.05}O_2$ powders post-treated at 700°C.

Fig. 4 shows the initial charge and discharge curves and cycling performance of the layered $LiNi_{0.8}Co_{0.15}Al_{0.05}O_2$ powders post-treated at 700°C in the potential range 2.8–4.5 V at a current density of 20 mA g^{-1}. The initial discharge capacity of the powders was 163 mAh g^{-1}, which decreased to 95 mAh g^{-1} after 50 cycles with a capacity retention of 58%. The $LiNi_{0.8}Co_{0.15}Al_{0.05}O_2$ powders

post-treated at 700°C showed poor cyclability because of their low crystallinity and more extensive aggregation between the powders, as shown in Figs. 2 and 3.

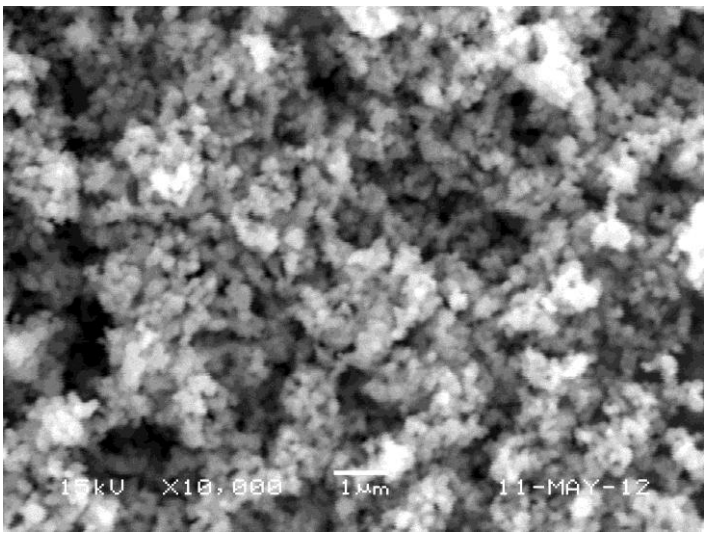

(a) SEM

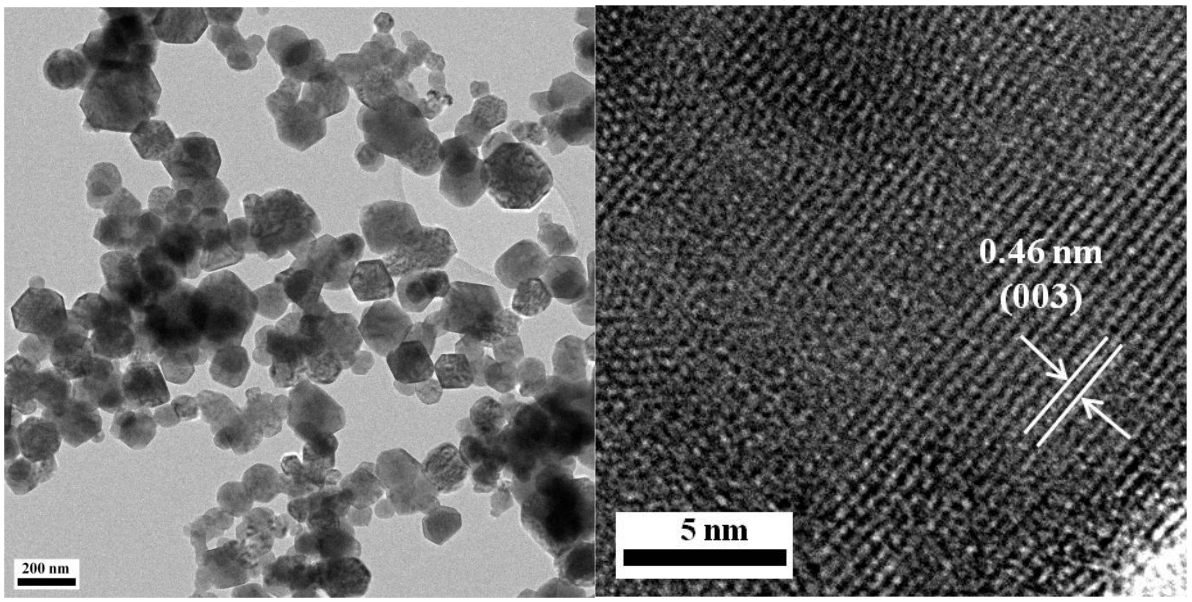

(b) TEM

Figure 5. SEM and TEM images of the $0.6Li_2MnO_3$-$0.4LiNi_{0.8}Co_{0.15}Al_{0.05}O_2$ composite powders post-treated at 700°C.

The layered–layered $0.6Li_2MnO_3 \cdot 0.4LiNi_{0.8}Co_{0.15}Al_{0.05}O_2$ composite powders exhibited morphology unlike that of the layered $LiNi_{0.8}Co_{0.15}Al_{0.05}O_2$ powders after post-treatment. Figs. 5 and 6 show the SEM and TEM images of the $0.6Li_2MnO_3 \cdot 0.4LiNi_{0.8}Co_{0.15}Al_{0.05}O_2$ composite powders post-treated at 700 and 800°C. The composite powders exhibited only a slightly aggregated morphology even at the high post-treatment temperature of 800°C. The mean sizes of the composite powders post-treated at 700 and 800°C measured from the TEM images were 127 and 180 nm, respectively. When two solid phases are mixed, each phase prevents the crystal growth in the other phase. All the post-

treated composite powders had polyhedral structures with clear crystal fringes. High-resolution TEM images exhibited clear lattice fringes with a separation of 0.46 nm.

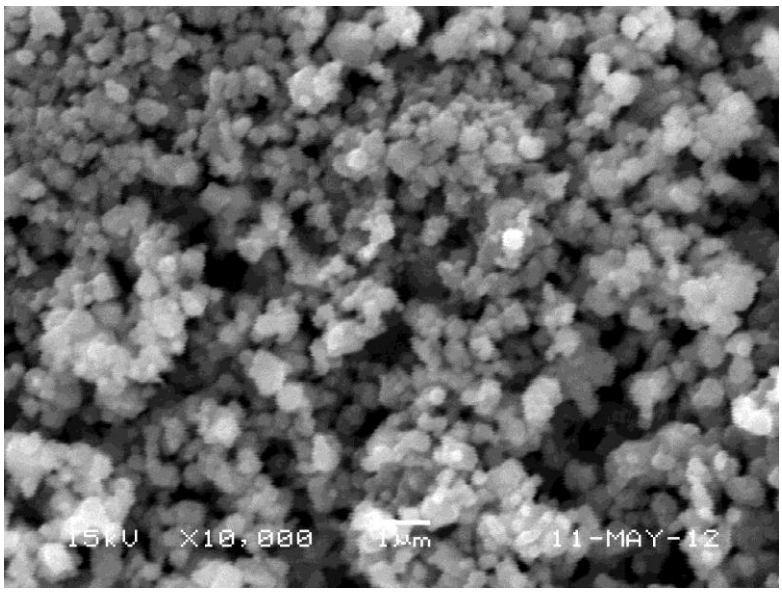

(a) SEM

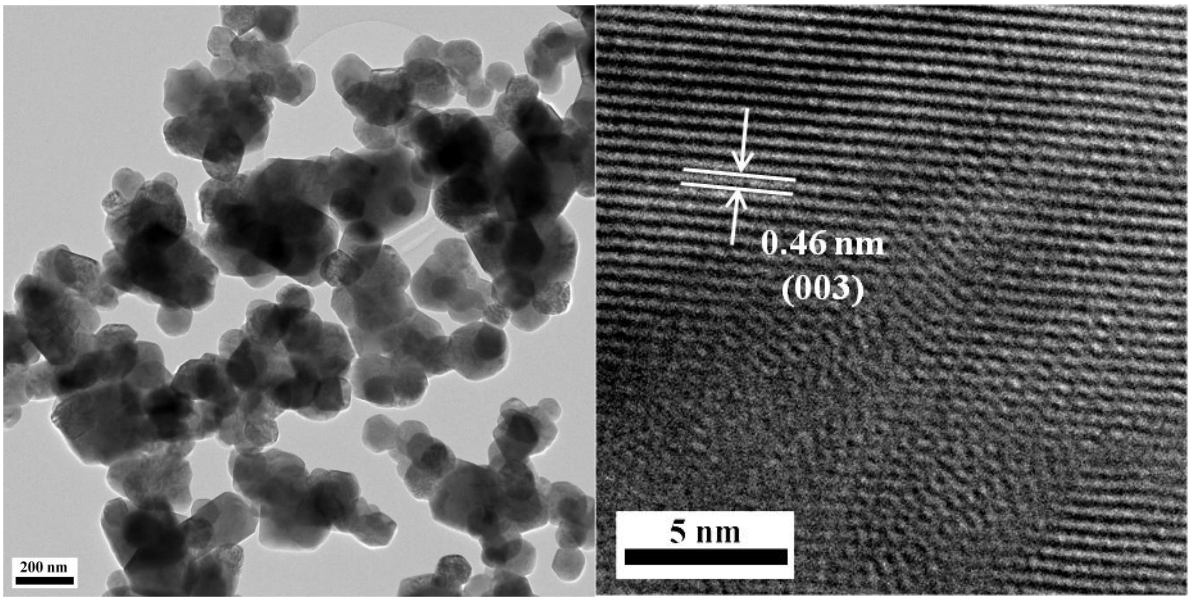

(b) TEM

Figure 6. SEM and TEM images of the $0.6Li_2MnO_3$-$0.4LiNi_{0.8}Co_{0.15}Al_{0.05}O_2$ composite powders post-treated at 800°C.

Fig. 7 shows the XRD patterns of the $0.6Li_2MnO_3 \cdot 0.4LiNi_{0.8}Co_{0.15}Al_{0.05}O_2$ composite powders post-treated at temperatures of 700 and 800°C. All the peaks corresponding to the post-treated composite powders can be indexed to a hexagonal α-$NaFeO_2$ structure, except for the peak near 21°, which is attributed to the superlattice structure of Li_2MnO_3 [12-14]. The (006)/(102) and (108)/(110) peaks were clearly split in the sample post-treated at 800°C. As the post-treatment temperature

increased up to 800°C, the sharpness and intensity of the XRD patterns of the composite powders increased. These results indicate that the mean crystallite size of the composite powders increased as the post-treatment temperature increased.

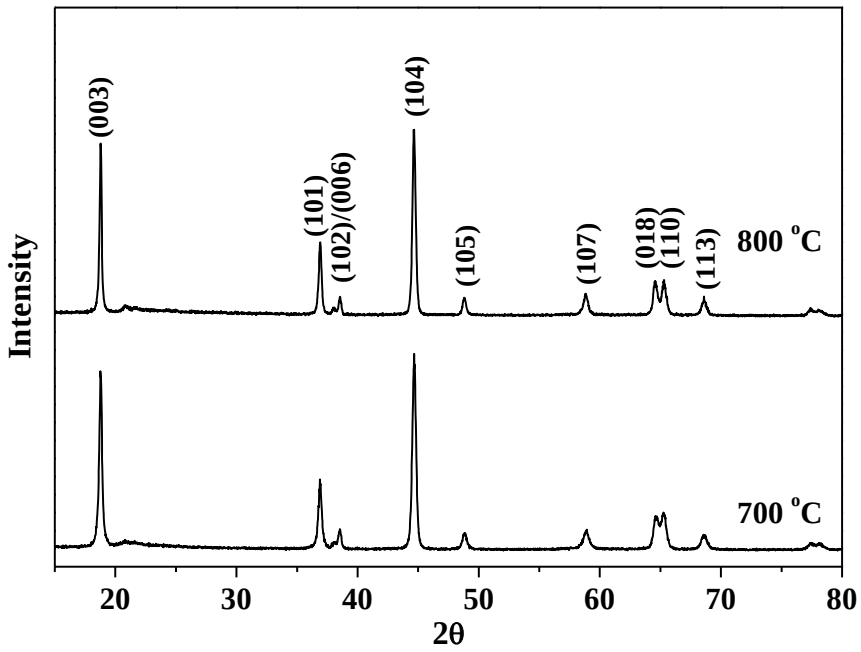

Figure 7. XRD patterns of the $0.6Li_2MnO_3$-$0.4LiNi_{0.8}Co_{0.15}Al_{0.05}O_2$ composite powders post-treated at 700 and 800°C.

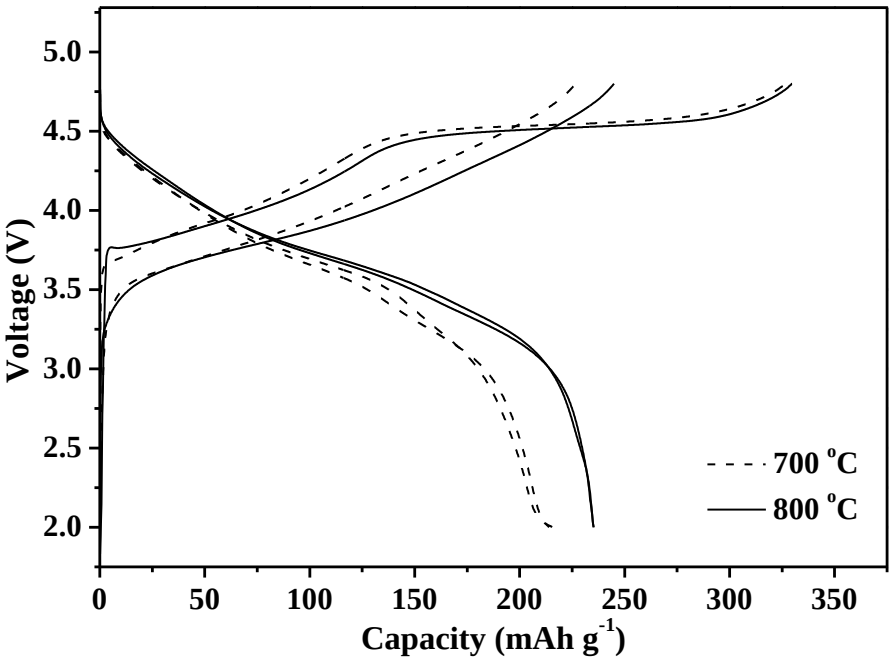

(a) Initial and second charge/discharge curves

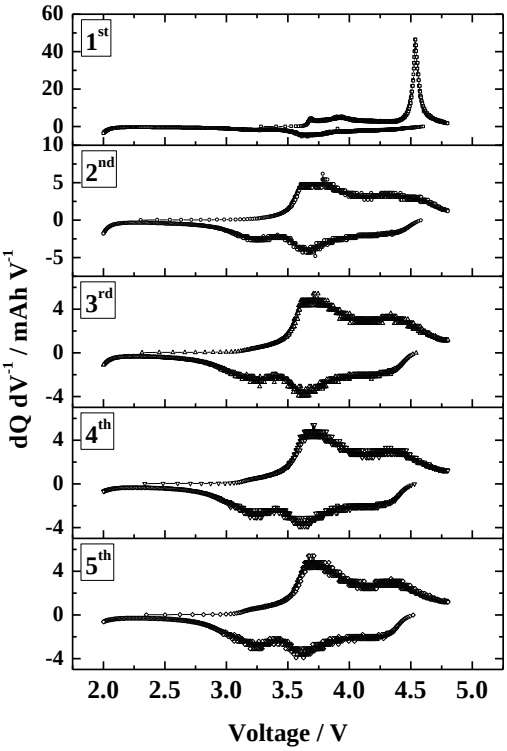

(b) *dQ/dV*, 700°C

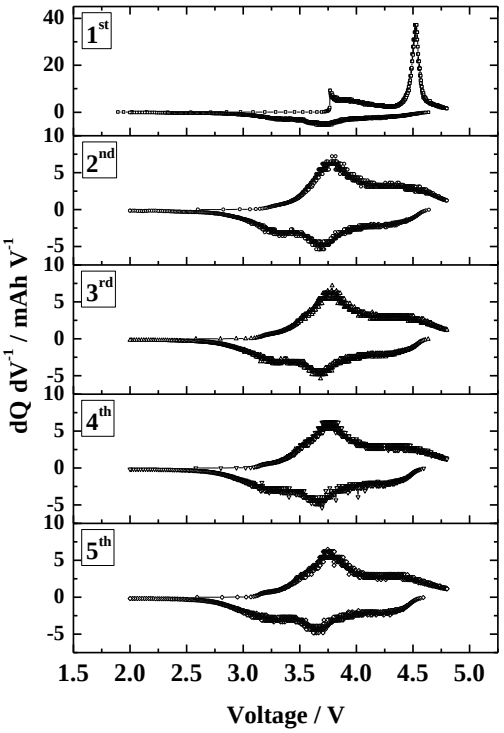

(c) *dQ/dV*, 800°C

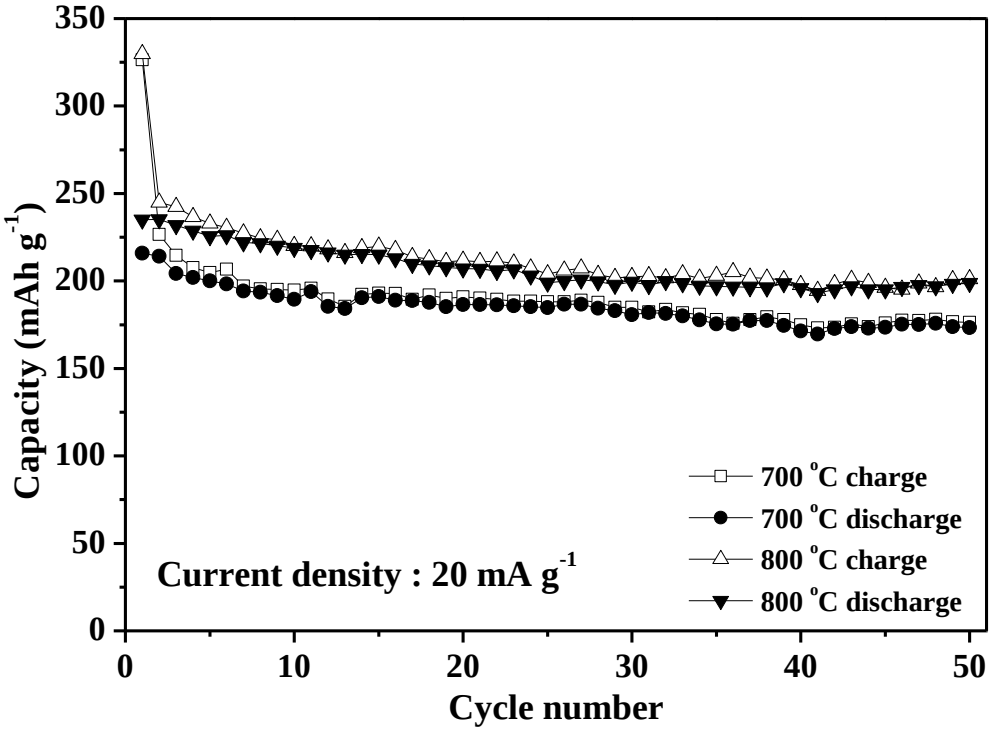

(d) Cycling performances

Figure 8. Cycling performances and *dQ/dV* curves of the $0.6Li_2MnO_3$-$0.4LiNi_{0.8}Co_{0.15}Al_{0.05}O_2$ composite powders post-treated at 700 and 800°C.

Fig. 8 show the cycling performances and differential capacity versus voltage (d*Q*/d*V*) curves of the composite powders post-treated at 700 and 800°C in the potential range 2–4.8 V at a current density of 20 mA g^{-1}. The smoothly sloping voltage profile below 4.5 V in the initial charge curve as shown in Fig. 8 (a) was due to the removal of Li from the layered $LiNi_{0.8}Co_{0.15}Al_{0.05}O_2$. The voltage plateau above 4.5 V was attributed to the removal of Li_2O from the Li_2MnO_3 component [28,29]. The voltage plateaus were not observed in the second charge curves of the composite powders post-treated at 700 and 800°C. The voltage plateaus around 4.5 V in the initial charge curve corresponded to the sharp oxidation peak in the d*Q*/d*V* curve, as shown in Fig. 8 (b) and (c). The first charge curve of the composite powders had two distinct oxidation peaks around 3.8 and 4.6 V. The peak at ~3.8 V was due to the oxidation of Ni^{2+} to Ni^{4+} [28,29]. The peak at ~4.6 V was due to the irreversible reaction involving the removal of lithium and oxygen as Li_2O from Li_2MnO_3 [28,29]. Two reduction peaks in the first discharge profile were present in the d*Q*/d*V* curves at ~3.3 and 3.8 V, corresponding to the $Mn^{4+/3+}$ and $Ni^{4+/2+}$ reductions, respectively [30,31]. The d*Q*/d*V* curves had similar shapes from the second cycles irrespective of the post-treatment temperatures of the composite powders. The composite powders post-treated at 700 and 800°C had similar initial charge capacities, as shown in Fig. 8 (d). However, the initial discharge capacities of the powders post-treated at 700 and 800°C were 216 and 235 mAh g^{-1}, respectively, in which the Coulombic efficiencies were 66 and 71%, respectively. The discharge capacities of the composite powders post-treated at 700 and 800°C after 50 cycles were 173 and 200 mAh g^{-1}, respectively, and the corresponding capacity retentions were 80 and 85%, respectively. The high crystallinity and phase homogeneity improved the electrochemical properties of the composite powders post-treated at 800°C.

4. CONCLUSIONS

The electrochemical and physical properties of layered–layered $0.6Li_2MnO_3 \cdot 0.4LiNi_{0.8}Co_{0.15}Al_{0.05}O_2$ composite powders were compared to those of layered $LiNi_{0.8}Co_{0.15}Al_{0.05}O_2$ powders prepared by high-temperature flame spray pyrolysis. The precursor powders had similar morphologies irrespective of the compositions of the cathode powders. The layered–layered composite powders were nanometer-sized with slightly aggregated structures even after post-treatment at high temperatures. On the other hand, the layered powders were micron-sized with hardly aggregated structures after post-treatment. Each phase of the composite powders prevented the crystal growth of the other phase. The layered–layered $0.6Li_2MnO_3 \cdot 0.4LiNi_{0.8}Co_{0.15}Al_{0.05}O_2$ composite nanopowders had higher initial discharge capacity and better cycle properties than those of the layered $LiNi_{0.8}Co_{0.15}Al_{0.05}O_2$ powders with sizes in the micron range.

ACKNOWLEDGEMENT
This work was supported by the National Research Foundation of Korea (NRF) grant funded by the Korea government (MEST) (No. 2012R1A2A2A02046367). This research was supported by Basic Science Research Program through the National Research Foundation of Korea (NRF) funded by the

Ministry of Education, Science and Technology (2012R1A1B3002382). This work was supported by Seoul R&BD Program (WR090671).

References

1. D. Liu, J. Han, J.B. Goodenough, *J. Power Sources*, 195 (2010) 2918.
2. B. Lin, Z. Wen, Z. Gu, S. Huang, *J. Power Sources*, 175 (2008) 564.
3. Y. Idemoto, Y. Takanashi, N. Kitamura, *J. Power Sources*, 189 (2009) 269.
4. T. Ogihara, H. Aikiyo, N. Ogata, K. Katayama, Y. Azuma, H. Okabe, T. Okawa, *Adv. Powder Technol.*, 13 (2002) 437.
5. S.H. Ju, Y.C. Kang, *Ceram. Int.*, 35 (2009) 1633.
6. Y.J. Wei, K. Nikolowski, S.Y. Zhan, H. Ehrenberg, S. Oswald, G. Chen, C.Z. Wang, H. Chen, *Electrochem. Commun.*, 11 (2009) 2008.
7. K.M. Begam, S.R.S. Prabaharan, *J. Power Sources*, 159 (2006) 319.
8. J.H. Kim, C.S. Yoon, Y.K. Sun, *J. Electrochem. Soc.*, 150 (2003) A538.
9. Z. Lu, J.R. Dahn, *J. Electrochem. Soc.*, 149 (2002) A815.
10. W.C. West, J. Soler, B.V. Ratnakumar, *J. Power Sources*, 204 (2012) 200.
11. F. Wu, H. Lu, Y. Su, N. Li, L. Bao, S. Chen, *J. Appl. Electrochem.*, 40 (2010) 783.
12. Z. Lu, L.Y. Beaulieu, A. Donaberger, C.L. Thomas, J.R. Dahn, *J. Electrochem. Soc.*, 149 (2002) A778.
13. M.M. Thackeray, S.H. Kang, C.S. Johnson, J.T. Vaughey, R. Benedek, S.A. Hackney, *J. Mater. Chem.*, 17 (2007) 3112.
14. Z. Lu, Z. Chen, J.R. Dahn, *Chem. Mater.*, 15 (2003) 3214.
15. A. Pramanik, C. Ghanty, S.B. Majumder, *Solid State Sci.*, 12 (2010) 1797.
16. A.D. Robertson, P.G. Bruce, *Electrochem. Solid-State Lett.*, 7 (2004) A294.
17. M.M. Thackeray, C.S. Johnson, J.T. Vaughey, N. Li, S.A. Hackney, *J. Mater. Chem.*, 15 (2005) 2257.
18. C.P. Grey, W.S. Yoon, J. Reed, G. Ceder, *Electrochem. Solid-State Lett.*, 7 (2004) A290.
19. T. Ohzuku, K. Ariyoshi, S. Yamamoto, *J. Ceram. Soc. Jpn.*, 110 (5) (2002) 501.
20. J.H. Kim, J.H. Yi, Y.N. Ko, Y.C. Kang, *Mater. Chem. Phys.*, 134 (2012) 254.
21. S.H. Choi, J.H. Kim, Y.N. Ko, Y.C. Kang, *Int. J. Electrochem. Sci*., 8 (2013) 1146.
22. W.Y. Teoh, R. Amal, L. Madler, *Nanoscale*, 2 (2010) 1324.
23. X. Zhang, H. Zheng, V. Battaglia, R.L. Axelbaum, *J. Power Sources*, 196 (2011) 3640.
24. J.H. Yi, J.H. Kim, H.Y. Koo, Y.N. Ko, Y.C. Kang, J.H. Lee, *J. Power Sources*, 196 (2011) 2858.
25. D.S. Jung, S.B. Park, Y.C. Kang, *Korean J. Chem. Eng.*, 27 (2010) 1621.
26. T.J. Patey, R. Buchel, S.H. Ng, F. Krumeich, S.E. Pratsinis, P. Novák, *J. Power Sources*, 189 (2009) 149.
27. T.J. Patey, R. Buchel, M. Nakayama, P. Novák, *Phys. Chem. Chem. Phys.*, 11 (2009) 3756.
28. C.S. Johnson, J.S. Kim, C. Lefief, N. Li, J.T. Vaughey, M.M. Thackeray, *Electrochem. Commun.*, 6 (2004) 1085.
29. S.H. Kang, P. Kempgens, S. Greenbaum, A.J. Kropf, K. Amine, M.M. Thackeray, *J. Mater. Chem.*, 17 (2007) 2069.
30. Y.J. Shin, W.J. Choi, Y.S. Hong, S. Yoon, K.S. Ryu, S.H. Chang, *Solid State Ionics*, 177 (2006) 515.
31. N. Yabuuchi, Y. Makimura, T. Ohzuku, *J. Electrochem. Soc.*, 154 (2007) A314.